

Energy spectra, wavefunctions and quantum diffusion for quasiperiodic systems

H. Q. Yuan,^{1,2,3} U. Grimm,¹ P. Repetowicz,¹ and M. Schreiber¹

¹*Institut für Physik, Technische Universität Chemnitz, 09107 Chemnitz, Germany*

²*Max-Planck-Institut für Chemische Physik fester Stoffe, Nöthnitzer Str. 40, 01187 Dresden, Germany*

³*Department of Physics, Xiangtan University, Xiangtan 411105, P. R. China*

(November 13, 2018)

Abstract

We study energy spectra, eigenstates and quantum diffusion for one- and two-dimensional quasiperiodic tight-binding models. As our one-dimensional model system we choose the silver mean or “octonacci” chain. The two-dimensional labyrinth tiling, which is related to the octagonal tiling, is derived from a product of two octonacci chains. This makes it possible to treat rather large systems numerically. For the octonacci chain, one finds singular continuous energy spectra and critical eigenstates which is the typical behaviour for one-dimensional Schrödinger operators based on substitution sequences. The energy spectra for the labyrinth tiling can, depending on the strength of the quasiperiodic modulation, be either band-like or fractal-like. However, the eigenstates are multifractal. The temporal spreading of a wavepacket is described in terms of the autocorrelation function $C(t)$ and the mean square displacement $d(t)$. In all cases, we observe power laws $C(t) \sim t^{-\delta}$ and $d(t) \sim t^\beta$. For the octonacci chain, $0 < \delta < 1$, whereas for the labyrinth tiling a crossover is observed from $\delta = 1$ to $0 < \delta < 1$ with increasing modulation strength. Corresponding to the multifractal eigenstates, we obtain anomalous diffusion with $0 < \beta < 1$ for both systems. Moreover, we find that the behaviour of $C(t)$ and $d(t)$ is independent of the shape and the location of the initial wavepacket. We use our results to check several relations between the diffusion exponent β and the fractal dimensions of energy spectra and eigenstates that were proposed in the literature.

PACS numbers: 71.23.Ft, 05.60.+w, 71.23.An, 71.30.+h

I. INTRODUCTION

Since the pioneering discoveries of quasicrystals with icosahedral,¹ dodecagonal,² decagonal,³ and octagonal⁴ symmetry, electronic transport phenomena arguably belong to the most celebrated and intriguing physical properties of these intermetallic alloys.^{5–7} For instance, the electric conductivity of icosahedral quasicrystals decreases strongly with decreasing temperature and with improving structural quality of the sample, and anomalous transport behaviour is also observed in other quantities such as thermopower or magnetoresistance. Stimulated by the experimental results, a lot of effort has been spent towards a better theoretical understanding of the transport phenomena in quasicrystalline materials.^{7–23} This is also of interest from the theoretical or mathematical point of view, because quasicrystals as ordered aperiodic structures are intermediate between periodically ordered crystals and short-range ordered amorphous solids. In particular, the anomalous diffusion of wave packets in quasiperiodic systems has attracted wide interest.^{14–23}

Multifractal eigenstates — neither extended over the system, nor exponentially localized — exist at the metal-insulator transition of the Anderson model of localization.^{24,25} In tight-binding models of quasicrystals, this kind of eigenstates has also been revealed.^{9–12,26} Generally, the energy spectra of one-dimensional (1D) quasicrystals are singular continuous.⁹ However, in higher-dimensional cases, the energy spectra can be band-like with finite measure, fractal-like with zero band width or a mixture of partly band-like and partly fractal-like character.^{12,13}

The diffusion properties of quasicrystals are associated with the complex eigenstates and energy spectra stated above.^{21–23} To describe the diffusion of a wave packet initially localized at some site n_0 , one usually discusses the temporal autocorrelation function^{14–18,27,28}

$$C(t) = \frac{1}{t} \int_0^t |\Psi_{n_0}(t')|^2 dt' \quad (1.1)$$

or the mean square displacement^{18–20,27}

$$d(t) = \left(\sum_n |\mathbf{r}_n - \mathbf{r}_{n_0}|^2 |\Psi_n(t)|^2 \right)^{1/2} \quad (1.2)$$

where $\Psi_n(t)$ is the amplitude of the wavefunction at time t at the n th site which is located at the position \mathbf{r}_n in space. Apparently, $C(t)$ is the time-averaged probability of a wave packet staying at the initial site at time t , and $d(t)$ determines the spreading of the width of a wave packet.

Generally, one finds $C(t) \sim t^{-\delta}$, $d(t) \sim t^\beta$ with $0 < \delta < 1$ and $0 < \beta < 1$ for 1D quasiperiodic systems.^{14,15,17–19} For higher-dimensional cases, no general results are available. Zhong *et al.*¹⁵ observed a transition of $C(t)$ with the increase of the quasiperiodic modulation strength in simple higher-dimensional Fibonacci lattices. For small patches of the octagonal tiling, Passaro *et al.*²⁰ found $d(t) \sim t^\beta$ with $0 < \beta < 1$ even for the case of a band-like spectrum. However, one of us obtained $C(t) \sim t^{-1}$ for this case after analyzing the long-time behaviour.¹⁶ In fact, it is quite difficult to derive the exact long-time behaviour of $C(t)$

and $d(t)$ from the investigation of rather small systems. Therefore, a study of a large higher-dimensional quasiperiodic system will be significant. In this paper, we will mainly discuss the diffusion properties on a 2D quasiperiodic tiling related to the octagonal quasicrystals. The tiling is based on the octonacci chain and thus permits us to study large systems.

Recent investigations show that the diffusion properties are connected with the multifractality of eigenstates and energy spectra.^{14–23,27–29} It can be rigorously proven that the exponent δ ruling the decay of the autocorrelation function $C(t)$ equals the correlation dimension D_2 of the local spectral measure associated with the initial site.^{14,15} In 1D quasiperiodic systems, Guarneri²¹ analytically deduced that $\beta \geq D_1$, where D_1 is the information dimension of the spectral measure. More recently, Ketzmerick *et al.*²³ argued that β is also related to the multifractal properties of the eigenstates. We shall address the question whether these relations exist in different quasiperiodic systems, especially in higher-dimensional cases.

This paper is organized as follows. In the next section, we describe the construction of the labyrinth tiling and its properties that are relevant for our analysis. Afterwards, in Sec. III, we consider a tight-binding model on the labyrinth tiling and express the eigenstates and eigenvalues in terms of eigenstates and eigenvalues of a tight-binding Hamiltonian on the octonacci chain. In Sec. IV we show the energy spectra and multifractal eigenstates for both these systems. Sec. V describes the diffusion properties of the octonacci chain. The diffusion properties of the labyrinth tiling will be emphasized in Sec. VI. In Sec. VII we discuss the fractal dimensions of eigenstates and eigenspectra and their relation to the diffusion properties. Finally, we conclude in Sec. VIII.

II. THE LABYRINTH TILING

The labyrinth tiling^{30,12} can be considered as a subset of the octagonal quasiperiodic tiling,³¹ and vice versa.¹² One can build it directly from the octonacci chain. In order to construct the labyrinth tiling, we introduce the octonacci sequence which can be produced by iterating the inflation rule

$$\varrho: \begin{array}{l} S \rightarrow L \\ L \rightarrow LSL \end{array} \quad (2.1)$$

on the initial word $w_0 = S$. The number of letters g_m in the m th iterate $w_m = \varrho^m(w_0)$ satisfies the recursion

$$g_m = 2g_{m-1} + g_{m-2}, \quad g_0 = g_1 = 1. \quad (2.2)$$

The numbers of letters L and S in w_m are given by f_m and f_{m-1} , respectively, which fulfill the same recursion relation with a different initial condition

$$f_m = 2f_{m-1} + f_{m-2}, \quad f_0 = 0, \quad f_1 = 1, \quad (2.3)$$

such that $g_m = f_m + f_{m-1}$. Their ratio in the limit sequence w_∞

$$\lim_{m \rightarrow \infty} \frac{f_m}{f_{m-1}} = \lim_{m \rightarrow \infty} \frac{g_m}{g_{m-1}} = \lambda \quad (2.4)$$

is given by the silver mean $\lambda = 1 + \sqrt{2}$ which is a root of the quadratic equation $\lambda^2 = 2\lambda + 1$. As can be seen from Eq. (2.2), g_m is odd for all m .

Associating with the letters S and L intervals of length 1 and λ , respectively, one obtains a linear chain \mathcal{C}_m of $N_m = g_m + 1$ sites, which is known as octonacci or silver mean chain.¹² We note that all words w_m obtained from the substitution rule (2.1) are palindromes, thus the resulting chains are symmetric under reflection.

The labyrinth tiling can be constructed from the Euclidean product $\mathcal{C}_m \times \mathcal{C}_m$ of two such chains. This product is a rectangular grid, thus its vertices can be classified into *even* and *odd* vertices if they can be reached from the origin by an *even* or *odd* number of steps along the bonds, respectively. This is completely analogous to the even and the odd sublattice of the square lattice. Connecting the *even* vertices by diagonal bonds, we obtain a finite approximant \mathcal{L}_m of the labyrinth tiling \mathcal{L} . The *odd* vertices, when connected by diagonal bonds, form another labyrinth tiling \mathcal{L}_m^* that is dual to \mathcal{L}_m . We note that, due to the palindromicity of w_m , \mathcal{L}_m and \mathcal{L}_m^* just differ by a 90 degree rotation.³² The finite labyrinth tiling \mathcal{L}_m consists of $N_m^2/2$ atoms. An example is shown in Fig. 1. By construction, the labyrinth tiling is symmetric with respect to reflection at the main diagonal. Taking this diagonal as the x axis and the direction orthogonal to it as the y axis, the coordinates of the vertices of the labyrinth tiling, labeled by $k, l \in \mathbb{Z}$, can be written as¹²

$$x_{k,l} = u_k + u_l \quad (2.5a)$$

$$y_{k,l} = u_k - u_l \quad (2.5b)$$

where the coordinates with *even* values of $k + l$ belong to \mathcal{L} , those with *odd* values of $k + l$ to \mathcal{L}^* . Here,

$$u_k = k/\sqrt{2} + \left[k/\sqrt{2} \right] \quad (2.6)$$

where $[x]$ denotes the integer closest to x . It is easy to see that the sequence of long and short lengths given by u_k again follows the octonacci sequence, but now the two intervals have lengths $(\lambda \pm 1)/2$ which again have ratio $(\lambda + 1)/(\lambda - 1) = \lambda$. Thus, the diagonal of the labyrinth $x_{k,k} = 2u_k$ is just a $\sqrt{2}$ -scaled version of the original octonacci sequence.

III. TIGHT-BINDING MODEL

The energy spectra for tight-binding Hamiltonians on the labyrinth tiling were investigated by Sire.¹² For properly chosen Hamiltonians, the analysis reduces to the one-dimensional case, and the energy spectrum can be derived directly from those of the corresponding Hamiltonian on the octonacci chain. However, the properties of eigenstates, which also factorize into the product of two eigenstates of the octonacci chain, were not discussed in Ref. 12. Here, we follow the same route to study the eigenvalues and eigenstates.

Consider two identical octonacci chains in the framework of a tight-binding model with zero on-site potentials

$$H^{(1)}\psi_k^{(1,i)} = t_k\psi_{k-1}^{(1,i)} + t_{k+1}\psi_{k+1}^{(1,i)} = E^{(1,i)}\psi_k^{(1,i)} \quad (3.1a)$$

$$H^{(2)}\psi_l^{(2,j)} = t_l\psi_{l-1}^{(2,j)} + t_{l+1}\psi_{l+1}^{(2,j)} = E^{(2,j)}\psi_l^{(2,j)} \quad (3.1b)$$

where superscripts (1) and (2) label the two chains and the indices i and j enumerate the eigenfunctions ψ and eigenvalues E of the two octonacci chains. Throughout the paper, we employ free boundary conditions, which formally corresponds to setting $\psi_0 = \psi_{N_m+1} = 0$. The hopping parameters t_k and t_l take values according to the octonacci sequence. We associate $t_{k,l} = 1$ to a *long* bond of length λ and $t_{k,l} = v$ to a *short* bond of length 1, respectively.

The eigenvalues of the octonacci chain are symmetric with respect to $E = 0$; if ψ is an eigenstate of H with eigenvalue E , then the state $\tilde{\psi}$ with amplitudes

$$\tilde{\psi}_k = (-1)^k \psi_k \quad (3.2)$$

is again an eigenstate, but has an eigenvalue $-E$. For $E = 0$, the eigenvalue equation reduces to the recursion

$$\psi_{k+1} = -\frac{t_k}{t_{k+1}} \psi_{k-1} \quad (3.3)$$

which always yields precisely *two* linearly independent solutions ψ^\pm which can be chosen to vanish on either *even* or *odd* sites. These have the form

$$\psi_{2r-1}^- = (-1)^{r-1} \psi_1^- \prod_{s=2}^r \frac{t_{2s-2}}{t_{2s-1}}, \quad \psi_{2r}^- = 0, \quad (3.4)$$

and

$$\psi_{2r-1}^+ = 0, \quad \psi_{2r}^+ = (-1)^{r-1} \psi_2^+ \prod_{s=2}^r \frac{t_{2s-1}}{t_{2s}}, \quad (3.5)$$

where $\psi_1^- \neq 0$ and $\psi_2^+ \neq 0$ are determined, up to phases, by normalization. We note that one has to be careful if one employs periodic boundary conditions because these, for an odd length of the chain, couple the even and odd sublattices of the chain. Thus, while there are again two states (3.4) and (3.5) for a periodic chain of even length, only a single state at $E = 0$ exists for an odd length of the chain.

Multiplying the two Eqs. (3.1a) and (3.1b), we obtain

$$\begin{aligned} H^{(1,2)} \Phi_{k,l}^{(i,j)} &= t_k t_l \Phi_{k-1,l-1}^{(i,j)} + t_k t_{l+1} \Phi_{k-1,l+1}^{(i,j)} + t_{k+1} t_l \Phi_{k+1,l-1}^{(i,j)} + t_{k+1} t_{l+1} \Phi_{k+1,l+1}^{(i,j)} \\ &= E^{(1,i)} E^{(2,j)} \Phi_{k,l}^{(i,j)} \end{aligned} \quad (3.6)$$

where we defined

$$\Phi_{k,l}^{(i,j)} = \psi_k^{(1,i)} \psi_l^{(2,j)} \quad (3.7)$$

as an eigenfunction on the product of the two chains with eigenvalue $E^{(1,i)} E^{(2,j)}$. In Eq. (3.6), only wave function amplitudes at positions $(k \pm 1, l \pm 1)$ contribute, thus the Hamiltonian $H^{(1,2)}$ corresponds to hopping along the *diagonals* of the product grid $\mathcal{C}_m \times \mathcal{C}_m$. The corresponding hopping parameters are the product of two hopping parameters in the octonacci chain and thus take values 1, v , and v^2 for diagonals of length $\lambda + 1$, $\sqrt{2\lambda + 2}$, and $\lambda - 1$, respectively.

Thus the system in Eq. (3.6) naturally separates into *two* independent sets of equations with $k+l$ *even* or $k+l$ *odd*, respectively. In this paper, we restrict our investigation to the case with $k+l$ even as the other case is completely analogous. Thus, $H^{(1,2)}$ can be interpreted as a tight-binding Hamiltonian with zero on-site potential defined on the labyrinth tiling \mathcal{L} . Clearly, the eigenvalues for the labyrinth are just products of the eigenvalues for the octonacci chain, and all such products appear as eigenvalues because the spectra of the two dual labyrinth tilings \mathcal{L}_m and \mathcal{L}_m^* are identical. For the corresponding eigenfunctions on \mathcal{L} , we have to construct linear combinations of the product eigenfunctions $\Phi_{i,j}$ (3.7) which vanish on the vertices of the dual tiling \mathcal{L}_m^* . This can be done as follows.

Suppose $\psi^{(1,i)}$ and $\psi^{(2,j)}$ are normalized eigenfunctions of the octonacci chain with eigenvalues $E^{(1,i)}$ and $E^{(2,j)}$, respectively. Then both $\Phi^{(i,j)} = \psi^{(1,i)}\psi^{(2,j)}$ and $\tilde{\Phi}^{(i,j)} = \tilde{\psi}^{(1,i)}\tilde{\psi}^{(2,j)}$ (3.2) are eigenfunctions of $H^{(1,2)}$ with the same eigenvalue $E^{(1,i)}E^{(2,j)}$, where we assume $E^{(1,i)} \neq 0$ and $E^{(2,j)} \neq 0$. But from Eq. (3.2) we have

$$\tilde{\Phi}_{k,l}^{(i,j)} = (-1)^{k+l}\Phi_{k,l}^{(i,j)} \quad (3.8)$$

and thus the linear combinations

$$\Psi^{(i,j)\pm} = \frac{1}{\sqrt{2}} \left(\Phi^{(i,j)} \pm \tilde{\Phi}^{(i,j)} \right) \quad (3.9)$$

are normalized eigenfunctions that vanish for *odd* or for *even* values of $k+l$, and thus on \mathcal{L}^* or \mathcal{L} , respectively. If one or both eigenvalues $E^{(1,i)}$ and $E^{(2,j)}$ are zero, we can make use of the previously discussed eigenfunctions ψ^+ (3.5) and ψ^- (3.4) to construct the desired wavefunctions. If one of the eigenvalues vanishes, say, without loss of generality, $E^{(1,i)} = 0$ and $E^{(2,j)} \neq 0$, the appropriate four linear combinations are

$$\Psi^{(i,j)\pm\pm} = \frac{1}{\sqrt{2}}\psi^{(1)\pm} \left(\psi^{(2,j)} \pm \tilde{\psi}^{(2,j)} \right) \quad (3.10)$$

where $\psi^{(1)\pm}$ is the wavefunction of Eqs. (3.5) and (3.4) on the first chain, and we also used the state $\tilde{\psi}^{(2,j)}$ which has an energy $-E^{(2,j)}$. Clearly, the wave functions $\Psi^{(i,j)++}$ and $\Psi^{(i,j)--}$ have support on \mathcal{L} , the other two linear combinations $\Psi^{(i,j)+-}$ and $\Psi^{(i,j)-+}$ live on \mathcal{L}^* . Finally, for $E^{(1,i)} = E^{(2,j)} = 0$, we have four states

$$\Psi^{(i,j)\pm\pm} = \psi^{(1)\pm}\psi^{(2)\pm} \quad (3.11)$$

where again $\Psi^{(i,j)++}$ and $\Psi^{(i,j)--}$ are supported on \mathcal{L} , and the remaining two product states $\Psi^{(i,j)+-}$ and $\Psi^{(i,j)-+}$ on \mathcal{L}^* . In particular, this argument proves that $E = 0$ is a $(2N_m - 2)$ -fold degenerate eigenvalue for the labyrinth \mathcal{L}_m . Thus we find, as for simple tight-binding Hamiltonians on the Penrose³³ or the octagonal Ammann-Beenker tiling, a large degeneracy of states in the ‘‘band’’ center at $E = 0$. However, in contrast to these well-known examples where the degeneracy stems from certain ‘‘confined’’ states³³ that occur as a consequence of the local topology of the tilings, the spectral measure carried by the states at $E = 0$ vanishes for the labyrinth as $N_m \rightarrow \infty$, thus it is not a finite fraction of the eigenstates that contributes to $E = 0$ in this case.

In practice, having the complete knowledge of the eigenstates for the labyrinth tiling at our disposal, we do not need to care too much about the precise linear combinations of states

derived above. Since the eigenvalues E_i , $i = 1, \dots, N$ of the octonacci chain are symmetric about zero, one can obtain the set of eigenvalues of the labyrinth tiling simply as

$$\{E_i E_j \mid 1 \leq i \leq \frac{N}{2}, j \leq i\} \cup \{E_i E_j \mid \frac{N}{2} < i \leq N, j \leq i - 1\} \quad (3.12)$$

where we assume that the eigenvalues of the octonacci chain are ordered as $E_i \geq E_j$ for $i > j$. The corresponding eigenvectors are most easily constructed by just restricting the products of eigenvectors to the sites of the labyrinth \mathcal{L} , and re-normalizing the resulting eigenstate. Eq. (3.2) guarantees that this procedure yields the correct results, because the states ψ and ψ just differ by an alternating sign.

IV. ENERGY SPECTRA AND WAVEFUNCTIONS

Following the results of Sec. III, one can easily calculate the density of states (DOS) and the integrated density of states (IDOS). For comparison, we show the DOS and the IDOS for the octonacci chain and the labyrinth tiling in Fig. 2. For the octonacci chain, the IDOS is a devil's staircase even for v close to 1 and the DOS is singular continuous with zero Lebesgue measure. By more detailed analysis, one finds a self-similar energy spectrum for the octonacci chain with a hierarchical gap structure as described by the gap labelling theorem.³⁴ In contrast, we observed a smooth IDOS without visual gaps as v approaches 1 in the labyrinth tiling. A more detailed analysis of the IDOS and the energy spectra shows that in the regime $0.6 < v < 1.0$ the energy spectrum contains no or a finite number of gaps; for $v < 0.6$ the spectrum is fractal-like and the IDOS is similar to a devil's staircase. Sire found that the spectrum is singular continuous with *finite* Lebesgue measure for $v \geq 0.4$,¹² which may indicate that the spectrum is a mixture of band-like and fractal-like parts in the regime $0.4 \leq v < 0.6$. In Fig. 2(b) one can see a peak at the center of the spectrum which is due to the degenerate states at $E = 0$. But it differs from the localized states observed in the Penrose tiling³³ in the sense that no leap at $E = 0$ is seen in the IDOS, in agreement with the results of the previous section. For varying parameter v , we find three regions with different behaviour of the DOS of the labyrinth tiling: a maximum around the center, distinct shoulders located between the spectral center and edge, and a tail at the band edge, which is similar to the behaviour observed for a tight-binding model on the icosahedral Ammann-Kramer tiling.¹¹

In order to characterize the eigenstates, we employ a multifractal analysis, which is based on the standard box-counting procedure.^{11,25} In our numerical calculations, we determine the singularity strength $\alpha(q)$ and the corresponding fractal dimension $f(q)$ by a linear regression procedure, but prior to this we need to check the linearity of $\sum_i \mu_i \ln \mu_i$ versus $\ln \varepsilon$, where $\mu_i(q, \varepsilon)$ denotes the normalized q th moment of the box probability for boxes of linear size εL . A homogeneously extended wave function corresponds to $\alpha(q) = f(q) = d$, where d denotes the spatial dimension. For critical eigenstates, the fractal dimension f is a smooth convex function of α , and α should be limited to a q -interval. Moreover, the generalized dimensions of the eigenstate ψ are given by $D_q^\psi = [f(q) - q\alpha(q)] / (1 - q)$ for $q \neq 1$ and $D_1^\psi = f(1) = \alpha(1)$.

The singularity spectra $f(\alpha)$ of eigenstates for both the octonacci chain and the labyrinth tiling show the typical shape expected for multifractal states, thus we refrain from showing

these here. For the octonacci chain, the eigenstates in the “band” center are more extended than those at the “band” edge. In this case, the curves $f(\alpha)$ become fairly narrow as v approaches 1. Generally, the eigenstates show stronger multifractal characteristics with decreasing parameter v . In contrast to the behaviour observed for the Penrose tiling,¹¹ for the labyrinth tiling we do not find that the multifractal behaviour of eigenstates becomes significantly stronger when moving from energies at the edge towards the center of the “band”. We also calculated the scaling behaviour of the inverse participation number

$$P^{-1}(E, V) = \sum_{\mathbf{r}} |\psi(\mathbf{r})|^4 \quad (4.1)$$

with respect to the size $V = L^d$ of the system,^{11,25} i.e.,

$$P^{-1}(E, V) \sim V^{-\gamma(E)} \quad (4.2)$$

for large V . A fractal eigenstate is characterized by $0 < \gamma < 1$, whereas $\gamma = 0$ corresponds to a localized state, and $\gamma = 1$ to an extended state. In general, the scaling exponent $\gamma(E)$ depends on the energy.²⁵ Numerically, one analyzes the scaling behaviour of $P^{-1}(E, V)$ at an energy E by averaging over the eigenstates within a small energy interval $E \pm \Delta E/2$. The result for eigenvectors from the center and at the lower edge of the spectrum is shown in Fig. 3 which corroborates the multifractal nature of the eigenstates in both systems. The exponent γ , given by the slope, decreases, presumably continuously, from $\gamma = 1$ for the periodic case $v = 1$ to $\gamma = 0$ for $v = 0$.

V. QUANTUM DIFFUSION FOR THE OCTONACCI CHAIN

In this short section, we briefly present our numerical results of the autocorrelation function $C(t)$ and the mean square displacement $d(t)$ for the octonacci chain. Further discussion and comparison with the results for the labyrinth will be given below.

Fig. 4 shows the autocorrelation function $C(t)$ of the octonacci chain. The initial site is located at the center of the system. The long-time behaviour of $C(t)$ follows $C(t) \sim t^{-\delta}$ with $0 < \delta < 1$ for different v . For small v , $C(t)$ displays strong oscillatory behaviour, which may result from level fluctuations. The result for $d(t)$ is displayed in Fig. 5. Evidently, $d(t) \sim t^\beta$ and β increases with increasing v , limited by $\beta < 1$. For a given modulation parameter v , we observe the relation $\beta > \delta$ between the two exponents. Similar results have been obtained for 1D Fibonacci chains and at the mobility edge of the Harper model.^{14,15,18,19} Therefore, in accordance with the singular continuous energy spectra and the multifractal eigenstates, the diffusion is usually anomalous in 1D quasiperiodic systems.

VI. QUANTUM DIFFUSION FOR THE LABYRINTH TILING

We now switch to the more interesting case of the labyrinth tiling. In Fig. 6, we show the behaviour of $C(t)$ for the labyrinth tiling. The number of sites in our system is $N^2/2 = 19\,602^2/2 = 192\,119\,202$, which is much larger than other 2D quasiperiodic systems discussed previously such as, for instance, Fibonacci lattices¹⁵ and the octagonal tiling.¹⁶ Therefore,

we can utilize this system to study the long-time behaviour of $C(t)$ more accurately than before. Apparently, Fig. 6 again exhibits a power law behaviour $C(t) \sim t^{-\delta}$. By a more detailed analysis, we surprisingly find a transition point at $v_c \approx 0.6$. For $v < v_c$ the slope of the curves decreases with decreasing v . In the regime $v > v_c$, the behaviour of $C(t)$ is the same as for a periodic system, i.e., $C(t) \sim t^{-1}$.¹⁵ When compared to the results of Sec. IV, we see that this regime corresponds to the region where one finds band-like energy spectra. Since δ equals the correlation dimension D_2 of the energy spectral measure,^{14,15} $\delta = 1$ is reasonable for the case of band-like spectra. Similar to the 1D case, one still has $0 < \delta < 1$ in the regime $v < v_c$ with fractal-like or mixed spectra for the labyrinth tiling. We expect that this is a general result for higher-dimensional quasiperiodic systems. Furthermore, we find the behaviour of $C(t)$ is independent of the initial site, which can be observed from the example shown in Fig. 6. Of course, as our analysis is based on numerical data for a finite system, we cannot possibly *prove* the existence of a true transition point v_c , because we cannot rule out a rapid, but continuous change in δ around $v \approx 0.6$.

The calculation of the square displacement $d(t)$ is numerically more expensive, thus we restrict ourselves to a smaller system of $N^2/2 = 578^2/2 = 167\,042$ sites. Nevertheless, this is still larger than the 2D octagonal quasicrystals studied previously.²⁰ In Fig. 7, we show that the long-time behaviour is described by a power law $d(t) \sim t^\beta$. In contrast to $C(t)$, we do not find a transition point for $d(t)$ as the parameter v is varied. As for the octagonal tiling²⁰ and for the octonacci chain, $0 < \beta < 1$ for the labyrinth tiling. Therefore, a band spectrum does not imply ballistic diffusion in quasicrystals. It can be argued that the exponent β is associated with the correlation dimension D_2^ψ of the eigenstates.²³ In 1D quasiperiodic systems, or at the metal-insulator transition in the Anderson model of localization, the eigenstates are multifractal^{9,24,25} and $0 < \beta < 1$.^{18,19,27} In accordance, the multifractal eigenstates in 2D quasicrystals may be expected to lead to anomalous diffusion with $0 < \beta < 1$. Possibly, ballistic diffusion can occur in 3D quasicrystals because their wavefunctions are more extended.¹¹

So far, we assumed that the initial wave packet is a δ -function, thus we start with an electron that is localized at a particular site $n_0 = (k_0, l_0)$ and follow the spreading of its wave function $\Psi^{\{n_0\}}$ with time. This means that, in general, *all* eigenstates contribute to the time evolution because the expansion in terms of the orthonormal basis of eigenstates $\Psi^{(i,j)}$ is

$$\Psi_{k,l}^{\{n_0\}} = \delta_{k,k_0} \delta_{l,l_0} = \sum_{i,j} \Psi_{k_0,l_0}^{(i,j)} \Psi_{k,l}^{(i,j)} \quad (6.1)$$

and thus the entire energy spectrum is probed. For convenience, we dropped the superscripts \pm on the wavefunctions of Eqs. (3.9)–(3.11), assuming that the proper linear combinations are used that are supported on the labyrinth \mathcal{L}_m . Note that we do not need a complex conjugation in Eq. (6.1) because the Hamiltonian is a real symmetric and we therefore can choose eigenvectors that form a real orthogonal matrix. In order to check for an energy dependence of the diffusion, we now consider different initial wave packets $\Psi^{\{n_0, [E - \frac{\Delta E}{2}, E + \frac{\Delta E}{2}]\}}$ which have a finite width and are constructed as linear combinations of eigenstates from a certain energy window $[E - \Delta E/2, E + \Delta E/2]$. The new normalized states can be written as

$$\Psi_{k,l}^{\{n_0, [E - \frac{\Delta E}{2}, E + \frac{\Delta E}{2}]\}} = \frac{\sum'_{i,j} \Psi_{k_0, l_0}^{(i,j)} \Psi_{k,l}^{(i,j)}}{\sqrt{\sum'_{i,j} |\Psi_{k_0, l_0}^{(i,j)}|^2}} \quad (6.2)$$

where the sum \sum' is restricted to the eigenstates $\Psi^{(i,j)}$ with eigenvalues $E^{(1,i)} E^{(2,j)} \in [E - \Delta E/2, E + \Delta E/2]$.³⁵ Clearly, Eq. (6.2) becomes Eq. (6.1) if the energy interval contains the complete spectrum, this is nothing but the usual completeness condition of the basis of eigenvectors.

We numerically checked different energy windows for the octonacci chain and the labyrinth tiling. Due to the high DOS around $E = 0$, we choose smaller intervals in the band center. The results in Fig. 8 and Fig. 9 show that the long-time behaviour of $C(t)$ and $d(t)$ hardly depends on the selection of the energy window. However, it is more complex at small times due to the different shapes and widths of the initial wave packets. The various values of $d(t)$ at the initial time reflect the width of the initial wave packet. The smaller the energy interval under consideration, the wider is the initial wavepacket. In practice, in order to avoid that the wave packet reaches the boundary too early, the energy interval may not be chosen too small.

VII. DYNAMICAL SCALING AND FRACTAL DIMENSIONS

In 1D quasiperiodic systems, it is known that the inequality $\beta \geq D_1$ relates the diffusion behaviour and the fractal properties of the energy spectrum.²¹ In d dimensions, this generalizes to the inequality $\beta \geq D_1/d$, thus it implies a superdiffusive behaviour $\beta \geq 1/2$ in two dimensions if $D_1 \geq 1$. In Fig. 10, the values of the exponent β for the octonacci chain and the labyrinth tiling are shown for various values of the parameter v . In all cases, we find that this inequality holds. Apparently, the diffusion exponents β for the octonacci chain and the labyrinth tiling are very close, which might be due to the product structure of the labyrinth and its wavefunctions.

According to a conjecture by Piéchon,²² $\beta = D_{-1}$ of the global spectral measure for one-dimensional quasiperiodic models with multifractal global spectral measure. In order to check this relation, we calculated D_{-1} , but it turns out that is rather difficult to extract the accurate values by a linear fit due to strong oscillations in the data. However, it appears that the relation does not hold for general parameter values v in the octonacci chain, and it certainly cannot be valid for the two-dimensional system as it only involves a dimension that characterizes the spectral measure.

Ketzmerick *et al.*²³ suggested an improved inequality $\beta \geq D_2/D_2^\psi$ which is numerically obeyed by 1D quasiperiodic models.²³ As can be seen from Fig. 10, this relation applies for the octonacci chain as well as for the the labyrinth tiling. However, in the two-dimensional case the inequality is less sharp as β is much larger than the ratio D_2/D_2^ψ , in particular for values of the parameter $v \geq 0.6$ where the energy spectrum is smooth and $D_2 \approx 1$.

For multifractal wavefunctions at the Anderson transition or at quantum Hall transitions, one finds $D_2^\psi = dD_2$ for a d -dimensional system.^{28,36} Above, it has been demonstrated that $D_2 = 1$ for the band-like spectra in 2D quasiperiodic systems, but the corresponding eigenstates are multifractal with generalized dimension $D_2^\psi < 2$. Although the eigenstates

of 2D quasiperiodic tight-binding models are similar to the critical states at the Anderson transition, the equality $D_2^\psi = dD_2$ apparently does not apply to 2D quasicrystals.

Recently, Zhong *et al.*²⁹ argued that one might interpret the superdiffusive behaviour in aperiodic systems as a ballistic behaviour in a space of effective dimension D_2^ψ , or that this should at least give an upper bound on the possible values of β . In Fig. 10, we compare the ratio D_2^ψ/d to β . It turns out that the values of β and D_2^ψ/d are rather close, but that there seems to be a systematic deviation with $\beta < D_2^\psi/d$ for small values of v and $\beta > D_2^\psi/d$ for v close to 1. Therefore, at least for large values of the parameter v , it appears that this bound does not hold.

Finally, we also included the values of D_1^ψ/d in Fig. 10, which apparently does give an upper bound on the values of β for the models under consideration. So far, this is just an observation, we cannot present an argument that this should hold in general.

VIII. CONCLUSION

In this paper, the energy spectra, wavefunctions and quantum diffusion for the octonacci chain and the labyrinth tiling are studied. The labyrinth tiling is based on the octonacci chain, which allows us to deal with very large systems. For the octonacci chain, the energy spectra are singular continuous and the eigenstates are critical. The energy spectra of the labyrinth tiling presumably are also singular continuous, but they can be band-like (i.e., of finite Lebesgue measure) with zero or finite gaps, a mixture of band-like and fractal parts, or fractal-like upon increasing the modulation strength. However, the eigenstates are multifractal irrespective of the value of the modulation parameter.

The propagation of an initial wave packet is discussed in terms of the autocorrelation function $C(t)$ and the mean square displacement $d(t)$. Numerical results show that $C(t) \sim t^{-\delta}$ and $d(t) \sim t^\beta$ for the octonacci chain and the labyrinth tiling. Corresponding to the multifractal eigenstates, we observe $0 < \beta < 1$ for both systems. In the case of fractal-like or mixed energy spectra and multifractal eigenstates, we find $0 < \delta < 1$. However, for a band-like spectrum, $C(t) \sim t^{-1}$ as in a periodic system, which causes a qualitative change of behaviour in $C(t)$ for the labyrinth tiling at a parameter value $v_c \approx 0.6$. Similar effects have also been observed for Fibonacci lattices¹⁵ and for the octagonal tiling.¹⁶

We believe that the anomalous diffusion shown in $d(t)$ and the crossover of the autocorrelation $C(t)$ will be a common phenomenon in 2D quasiperiodic systems. Of course, to observe the crossover in $C(t)$ one needs a parameter that allows one to continuously move away from the periodic case, which is not easily at hand for the most commonly investigated quasiperiodic model systems such as the Penrose or the octagonal tiling. Finally, we also studied the influence of different initial wave packets by choosing the eigenstates from various energy windows. The results show that the behaviour of $C(t)$ and $d(t)$ does not depend significantly on the shape and the location of the initial wave packet.

Comparing the values of β with several expressions involving the fractal dimensions of energy spectra and eigenstates that were proposed in the literature, we find that the inequality $\beta \geq D_2/D_2^\psi$ of Ref. 23 holds true. However, it seems that the bound $\beta \leq D_2^\psi/d$ proposed recently by Zhong *et al.*²⁹ may be violated for parameter values v close to one, i.e., close to the periodic case. However, we find that the weaker condition $\beta \leq D_1^\psi/d$ is always satisfied.

Our present work corroborates that there are strong relations between fractal properties of energy spectra and wavefunctions on the one hand and the exponents describing the quantum diffusion on the other hand. However, it appears to be difficult to find relations that give quantitative agreement for one- and two-dimensional aperiodic systems. Here, a deeper understanding of the underlying physics is desirable. Higher-dimensional systems constructed as products of one-dimensional systems, such as the labyrinth tiling, provide useful toy examples for further investigations which can, at least, be treated numerically in an efficient way.

ACKNOWLEDGMENTS

The authors thank J. X. Zhong for fruitful discussions. HQY is grateful for the kind hospitality in Chemnitz. Financial support from DFG (UG) and the NSF of China (HQY) is gratefully acknowledged.

REFERENCES

- ¹ D. Shechtman, I. Blech, D. Gratias, and J.W. Cahn, Phys. Rev. Lett. **53**, 1951 (1984).
- ² T. Ishimasa, H.-U. Nissen, and Y. Fukano, Phys. Rev. Lett. **55**, 511 (1985).
- ³ L. Bendersky, Phys. Rev. Lett. **55**, 1461 (1985).
- ⁴ N. Wang, H. Chen, and K. H. Kuo, Phys. Rev. Lett. **59**, 1010 (1987).
- ⁵ S. J. Poon, Adv. in Phys. **41**, 303 (1992).
- ⁶ C. Berger, in *Lectures on Quasicrystals*, edited by F. Hippert and D. Gratias (Les Éditions de Physique, Les Ulis, 1994), pp. 463–504.
- ⁷ C. Janot and R. Mosseri, Proceedings of the 5th International Conference on Quasicrystals (World Scientific, Singapore, 1995).
- ⁸ S. Roche, G. Trambly de Laissardière, and D. Mayou, J. Math. Phys. **38**, 1794 (1997).
- ⁹ Q. Niu and F. Nori, Phys. Rev. Lett. **57**, 2057 (1986); C. Tang and M. Kohmoto, Phys. Rev. B **34**, 2041 (1986); M. Kohmoto, B. Sutherland, and C. Tang, Phys. Rev. B **35**, 1020 (1987); T. Fujiwara, M. Kohmoto, and T. Tokihiro, Phys. Rev. B **40**, 7413 (1989); J. Bellissard, B. Iochum, E. Scoppola, and D. Testard, Commun. Math. Phys. **125** 527 (1989); Q. Niu and F. Nori, Phys. Rev. B **42**, 10329 (1990); J. X. Zhong, J. Bellissard, and R. Mosseri, J. Phys.: Condens. Matter **7**, 3507 (1995).
- ¹⁰ B. Sutherland, Phys. Rev. B **34**, 3904 (1986); Y. Liu and P. Ma, Phys. Rev. B **43**, 1378 (1991).
- ¹¹ T. Rieth and M. Schreiber, J. Phys.: Condens. Matter **10**, 783 (1998); T. Rieth, U. Grimm, and M. Schreiber, in *Proceedings of the 6th International Conference on Quasicrystals*, edited by S. Takeuchi and T. Fujiwara (World Scientific, Singapore, 1998), pp. 639–42.
- ¹² C. Sire, Europhys. Lett. **10**, 483 (1989); C. Sire, in *Lectures on Quasicrystals*, edited by F. Hippert and D. Gratias (Les Editions de Physique, Les Ulis, 1994), pp. 505–33.
- ¹³ T. Odagaki and D. Nguyen, Phys. Rev. B **33**, 2184 (1986); K. Ueda and H. Tsunetsugu, Phys. Rev. Lett. **58**, 1272 (1987); J. A. Ashraff, J.-M. Luck, and R. B. Stinchcombe, Phys. Rev. B **41**, 4314 (1990); V. G. Benza and C. Sire, Phys. Rev. B **44**, 10343 (1991); J. X. Zhong and R. Mosseri, J. Phys. (France) I **4**, 1513 (1994).
- ¹⁴ R. Ketzmerick, G. Petschel, and T. Geisel, Phys. Rev. Lett. **69**, 695 (1992).
- ¹⁵ J. X. Zhong and R. Mosseri, J. Phys.: Condens. Matter **7**, 8383 (1995).
- ¹⁶ H. Q. Yuan and J. X. Zhong, Acta Physica Sinica (Overseas Edition) **7**, 196 (1998).
- ¹⁷ C. R. de Oliveira and G. Q. Pellegrino, J. Phys. A: Math. Gen. **32**, L285 (1999).
- ¹⁸ S. D. Evangelou and D. E. Katsanos, J. Phys. A: Math. Gen. **26**, L1243 (1993).
- ¹⁹ H. Hiramoto and S. Abe, J. Phys. Soc. Jpn. **57**, 230 (1988); H. Hiramoto and S. Abe, J. Phys. Soc. Jpn. **57**, 1365 (1988); T. Geisel, R. Ketzmerick, and G. Petschel, Phys. Rev. Lett. **66**, 1651 (1991); M. Wilkinson and E. J. Austin, Phys. Rev. B **50**, 1420 (1994).
- ²⁰ B. Passaro, C. Sire, and V. G. Benza, Phys. Rev. B **46**, 13751 (1992).
- ²¹ I. Guarneri, Europhys. Lett. **10**, 95 (1989); I. Guarneri, Europhys. Lett. **21**, 729 (1993).
- ²² F. Piéchon, Phys. Rev. Lett. **76**, 4372 (1996).
- ²³ R. Ketzmerick, K. Kruse, S. Kraut, and T. Geisel, Phys. Rev. Lett. **79**, 1959 (1997); and references therein.
- ²⁴ M. Schreiber and H. Grussbach, Phys. Rev. Lett. **67**, 607 (1991); T. Terao, Phys. Rev. B **56**, 975 (1997).
- ²⁵ A. Eilmes, R. A. Römer, and M. Schreiber, Eur. Phys. J. B **1**, 29 (1998).
- ²⁶ P. Repetowicz, U. Grimm, and M. Schreiber, Phys. Rev. B **58**, 13482 (1998).

- ²⁷ T. Kawarabayashi and T. Ohtsuki, Phys. Rev. B **53**, 6975 (1996); T. Ohtsuki and T. Kawarabayashi, J. Phys. Soc. Jpn. **66**, 314 (1997).
- ²⁸ B. Huckestein and L. Schweitzer, Phys. Rev. Lett. **72**, 713 (1994).
- ²⁹ J. X. Zhong, Z. Y. Zhang, M. Schreiber, E. W. Plummer, and Q. Niu, Dynamical scaling properties of electrons in quantum systems with multifractal eigenstates (preprint).
- ³⁰ C. Sire, R. Mosseri, and J.-F. Sadoc, J. Phys. (France) **50**, 3463 (1989).
- ³¹ R. Ammann, B. Grünbaum, and G. C. Shephard, Discrete Comput. Geom. **8**, 1 (1992); M. Duneau, R. Mosseri, and C. Oguey, J. Phys. A: Math. Gen. **22**, 4549 (1989).
- ³² M. Baake, U. Grimm, and R. J. Baxter, Int. J. Mod. Phys. B **8**, 3579 (1994).
- ³³ M. Kohmoto and B. Sutherland, Phys. Rev. Lett. **56**, 2740 (1986); T. Fujiwara, M. Arai, T. Tokihiro, and M. Kohmoto, Phys. Rev. B **37** 2797 (1988); M. Arai, T. Tokihiro, T. Fujiwara, and M. Kohmoto, Phys. Rev. B **38** 1621 (1988); T. Rieth and M. Schreiber, Phys. Rev. B **51**, 15827 (1995).
- ³⁴ J. Bellissard, A. Bovier, and J. M. Ghez, Rev. Math. Phys. **4** 1 (1992); M. Baake, U. Grimm, and D. Joseph, Int. J. Mod. Phys. B **7** 1527 (1993).
- ³⁵ L. Schweitzer, J. Phys.: Condens. Matter **7**, L281 (1995).
- ³⁶ B. Huckestein and R. Klesse, Phys. Rev. B **55**, R7303 (1997).

FIGURES

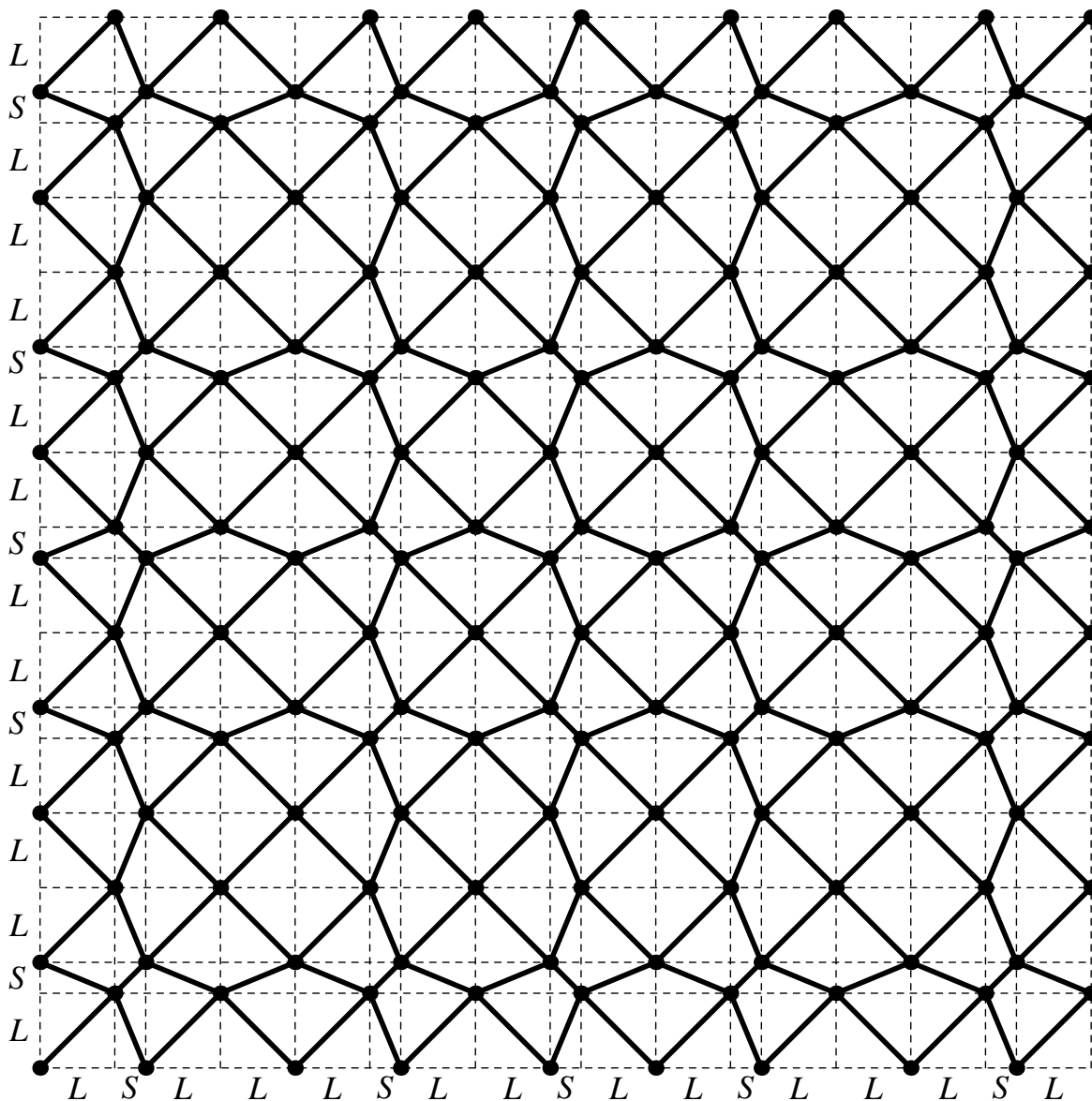


FIG. 1. The labyrinth tiling \mathcal{L}_4 . The dashed lines represent the product $\mathcal{C}_4 \times \mathcal{C}_4$.

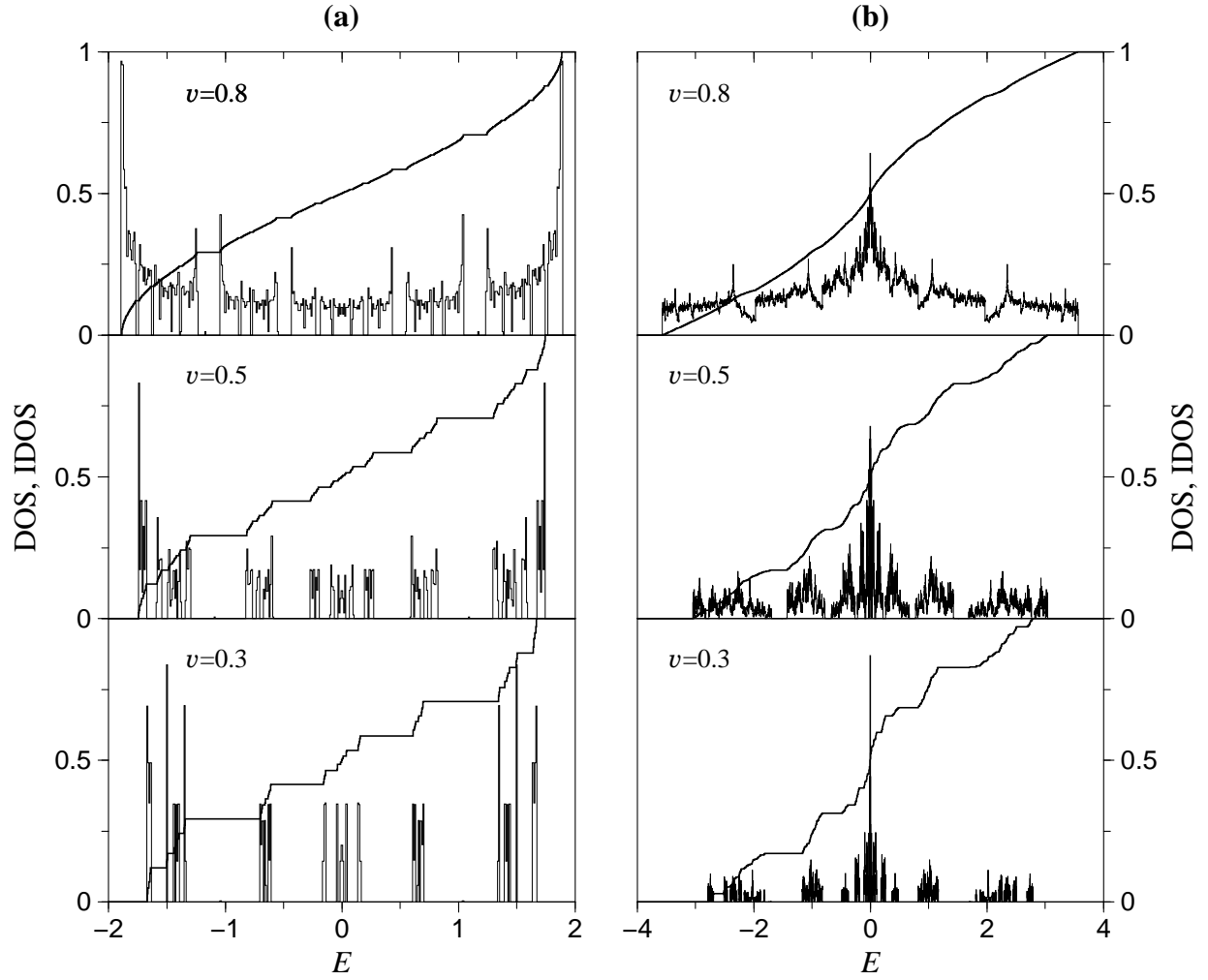


FIG. 2. The DOS (arbitrary scale) and the IDOS (bold line) for various hopping parameters ν for (a) the octonacci chain, and (b) the labyrinth tiling.

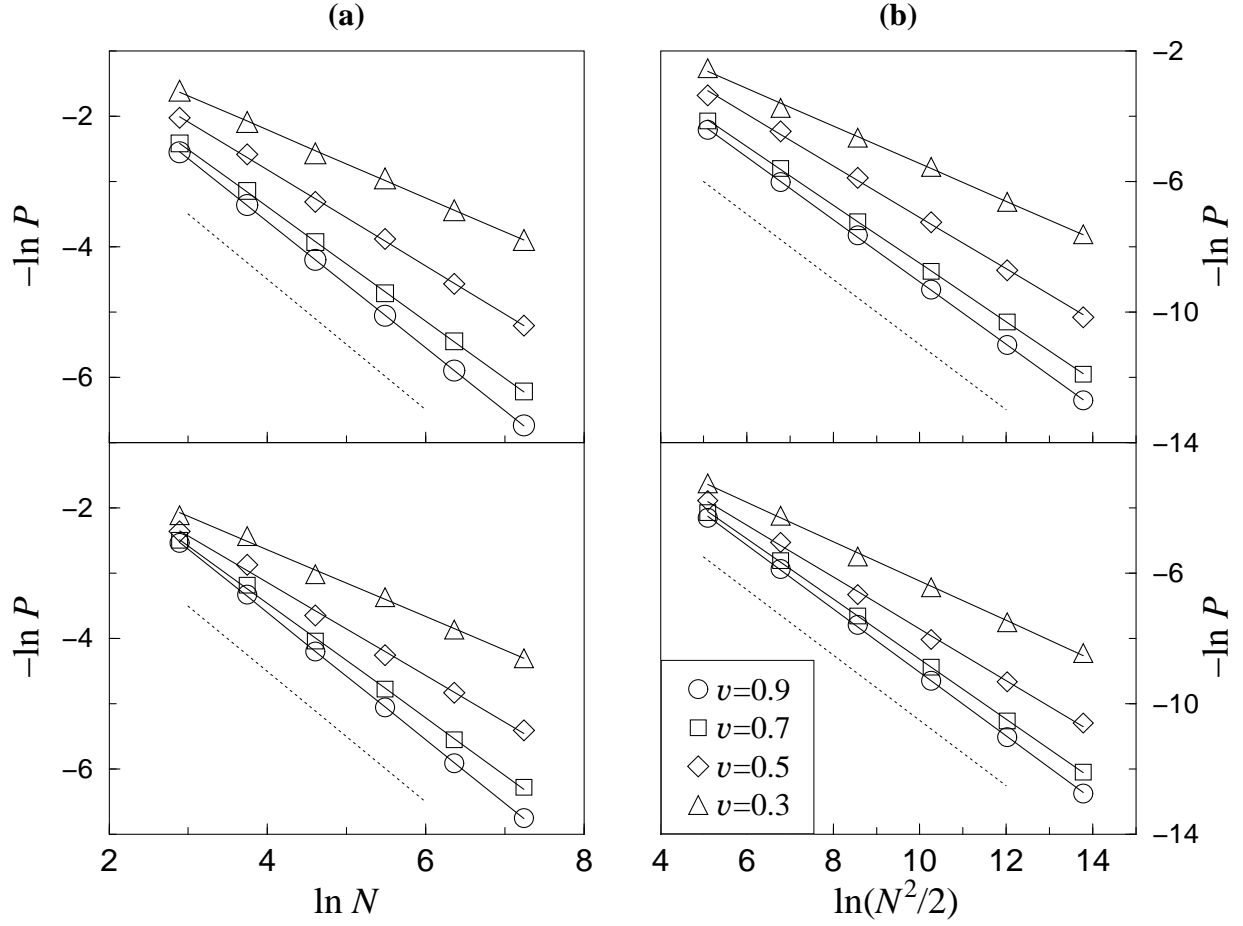


FIG. 3. The dependence of the inverse participation numbers $P^{-1}(E, V)$ on the size V of (a) the octonacci chain, and (b) the labyrinth tiling, for $E = 0$ (top) and $E = E_{\min}$ (bottom). Lines are least-squares fits to the data, the dotted lines correspond to $P^{-1}(E, V) \sim V^{-1}$.

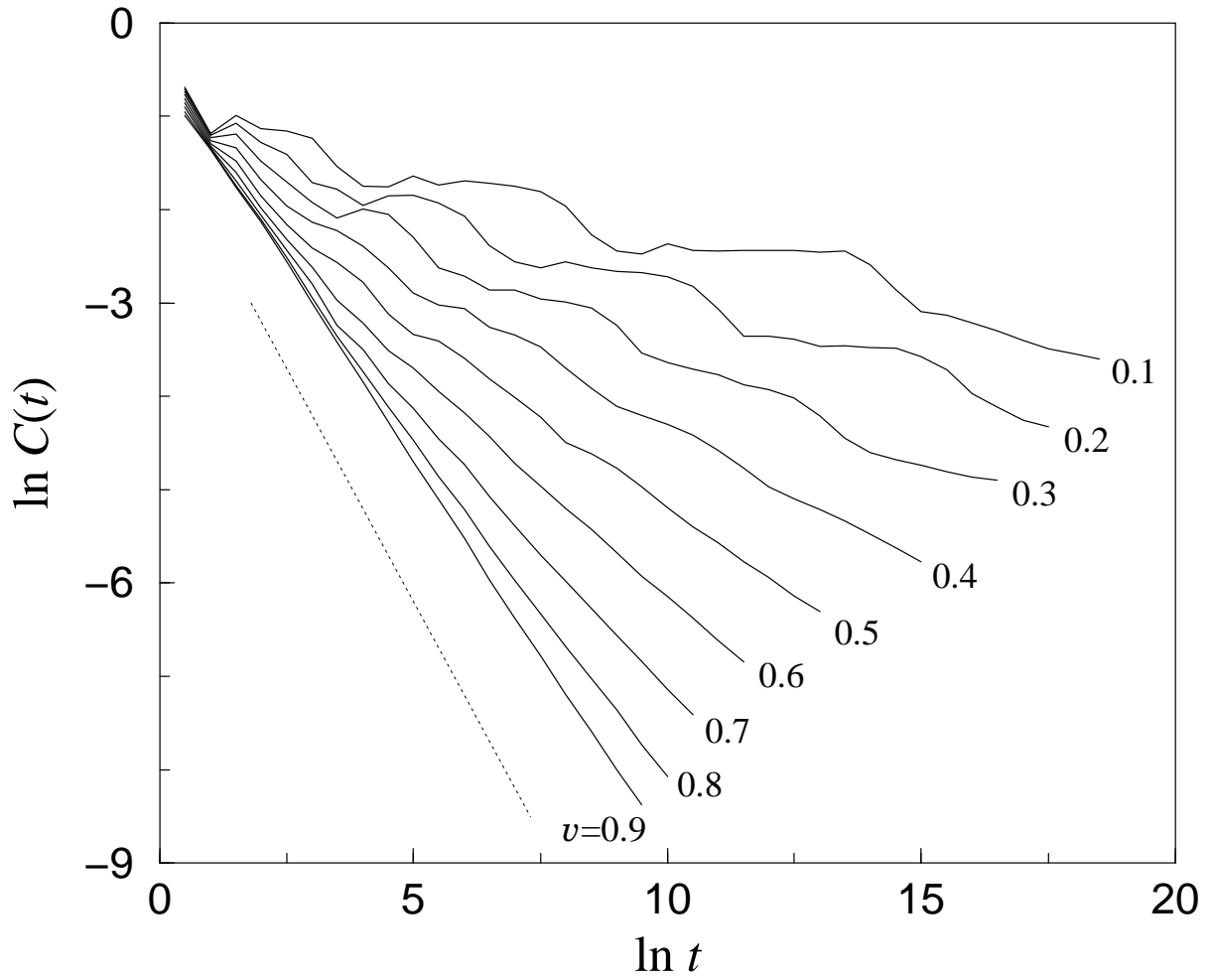


FIG. 4. The autocorrelation function $C(t)$ for the octonacci chain with $N = 19602$ and initial site $n_0 = 9801$. The dotted line corresponds to $C(t) \sim t^{-1}$.

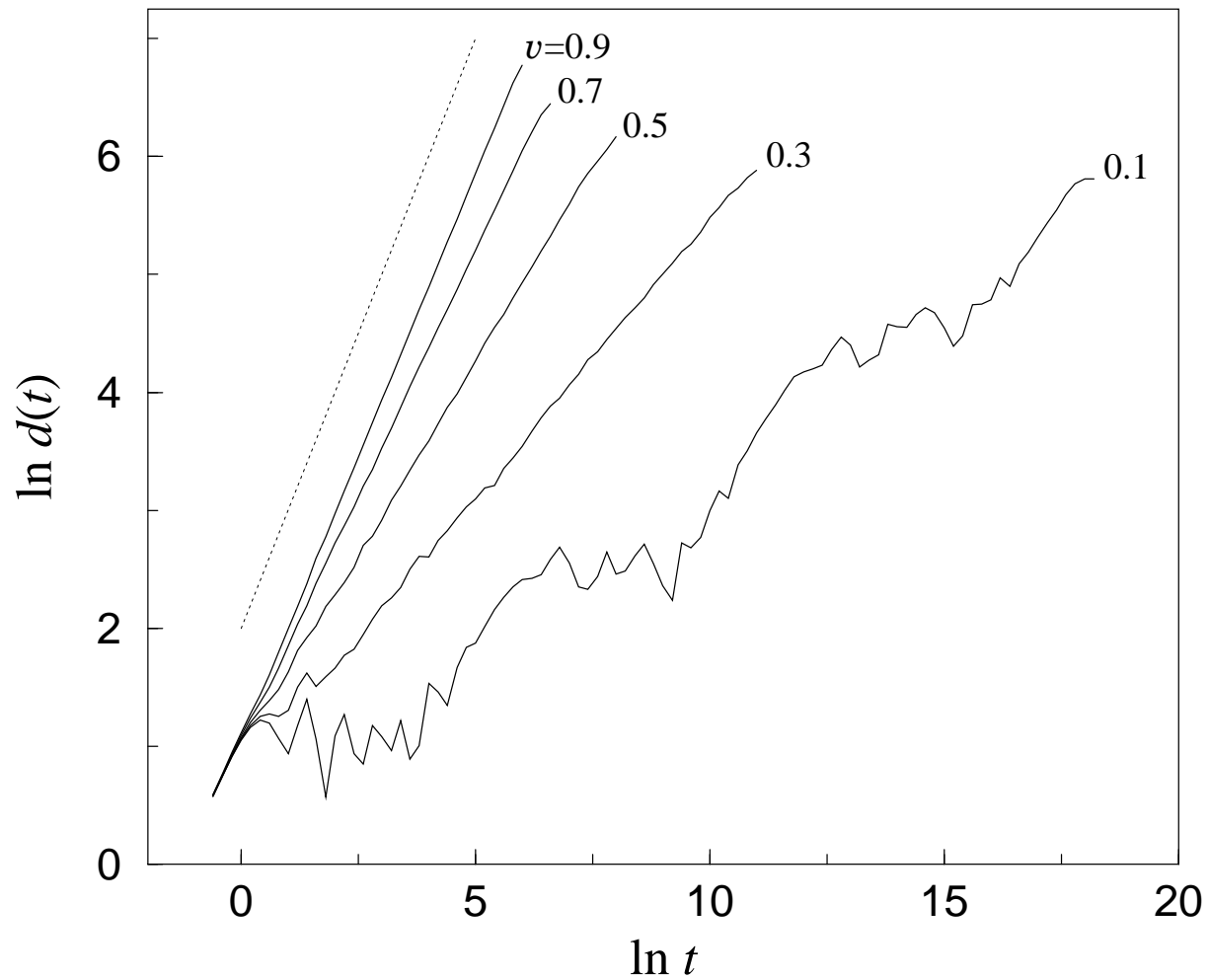


FIG. 5. The mean square displacement $d(t)$ for the octonacci chain with $N = 1394$ and initial site $n_0 = 697$. The dotted line corresponds to ballistic motion $d(t) \sim t$.

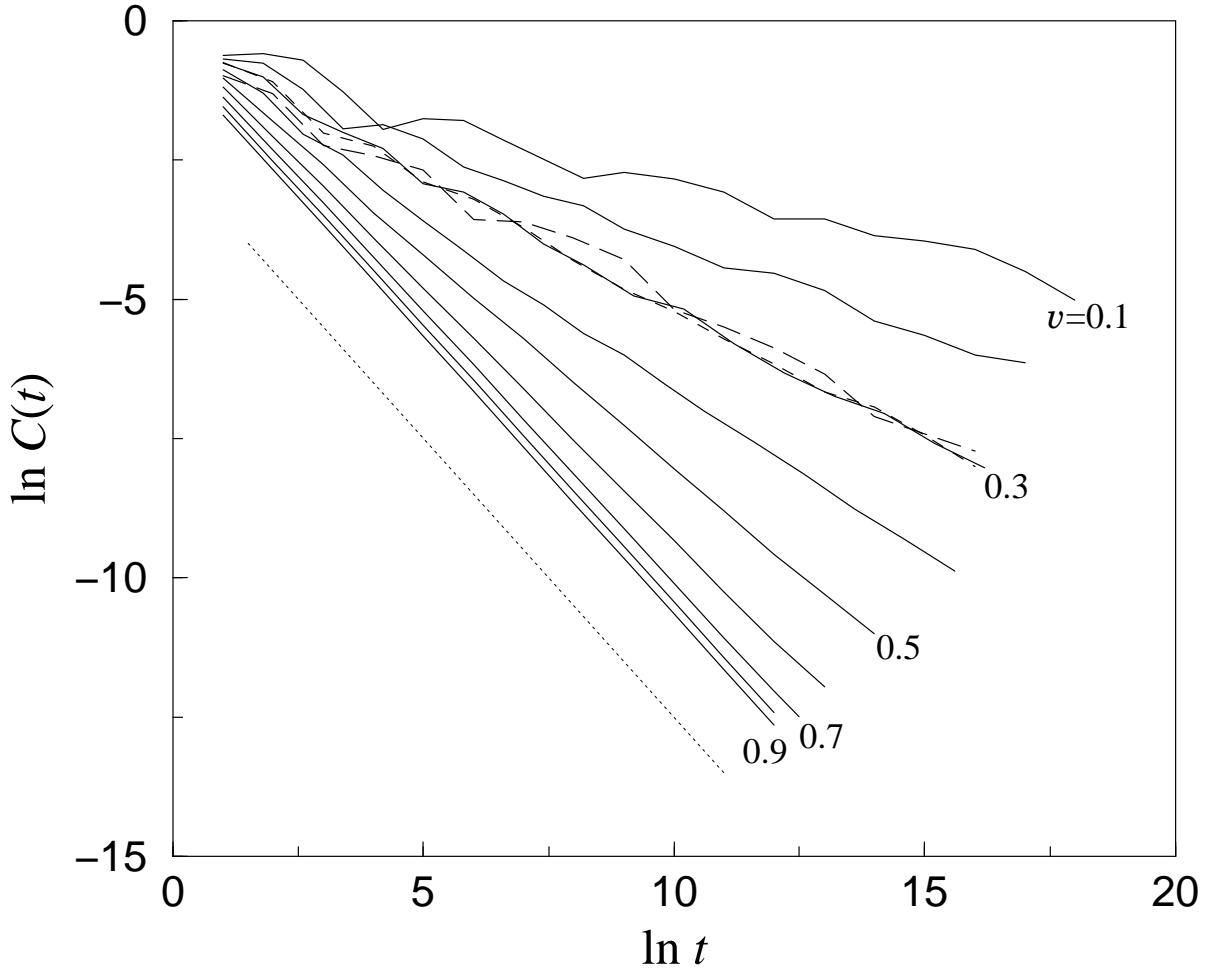


FIG. 6. The autocorrelation function $C(t)$ for the labyrinth tiling with $v = 0.1, 0.2, \dots, 0.9$. The system size is $N^2/2 = 19\,602^2/2 = 192\,119\,202$, and the initial site is $n_0 = (9800, 9800)$. For $v = 0.3$, the two dashed lines correspond to different choices of the initial site n_0 . The dotted line shows $C(t) \sim t^{-1}$.

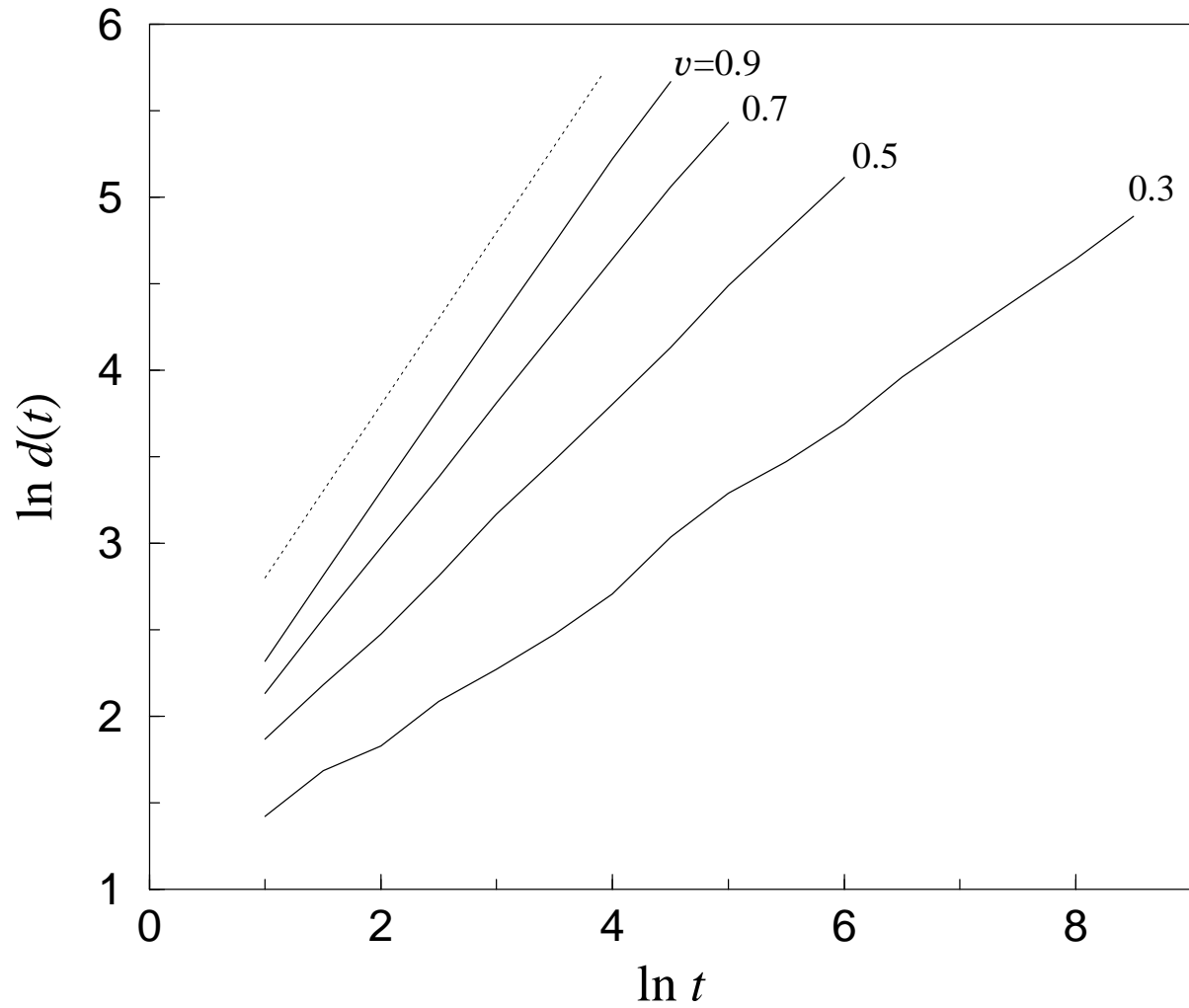


FIG. 7. The mean square displacement $d(t)$ for the labyrinth tiling shows $d(t) \sim t^{-\beta}$ with $\beta = 0.95, 0.83, 0.66,$ and 0.47 for $v = 0.9, 0.7, 0.5,$ and 0.3 , respectively. The dotted line corresponds to ballistic motion $d(t) \sim t$.

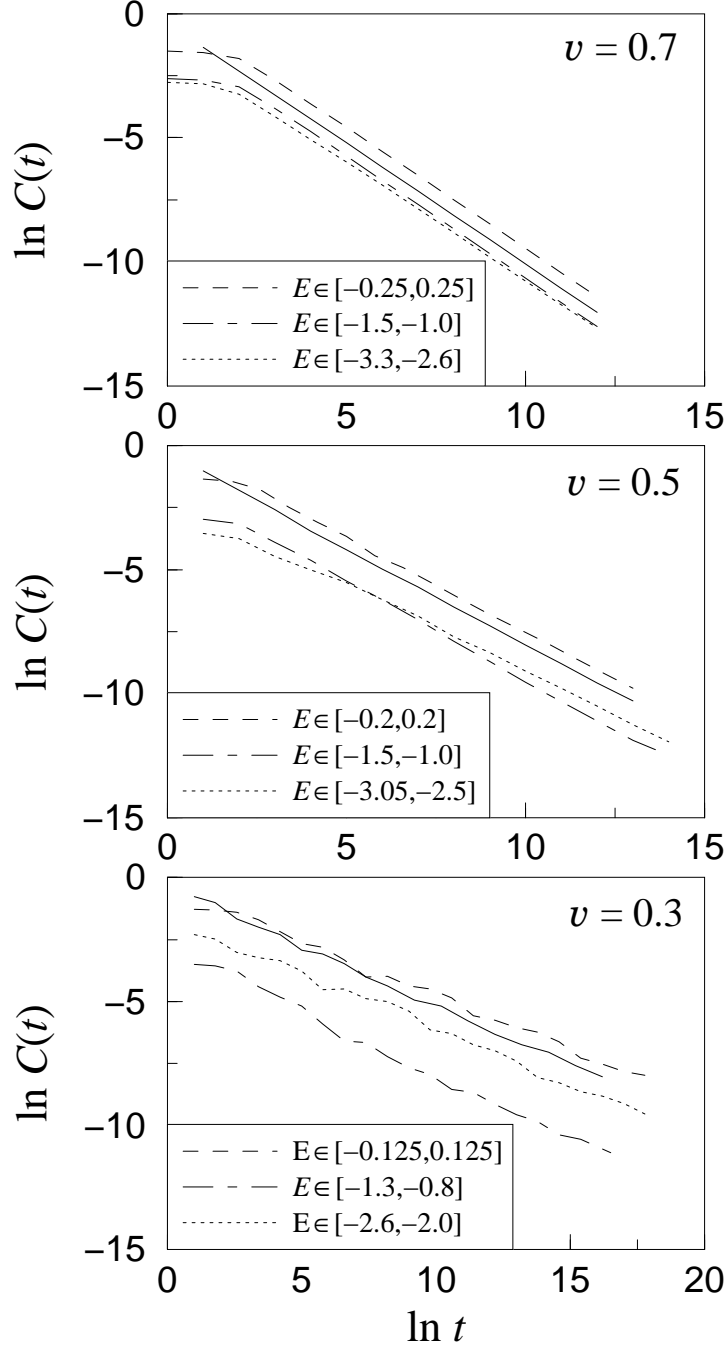


FIG. 8. The dependence of autocorrelation function $C(t)$ on various energy windows. The energy windows are arbitrarily chosen from the band center (dashed line), the band edge (dotted line) and between the band center and the band edge (dot-dashed line), respectively. The solid line is the result for the full spectrum.

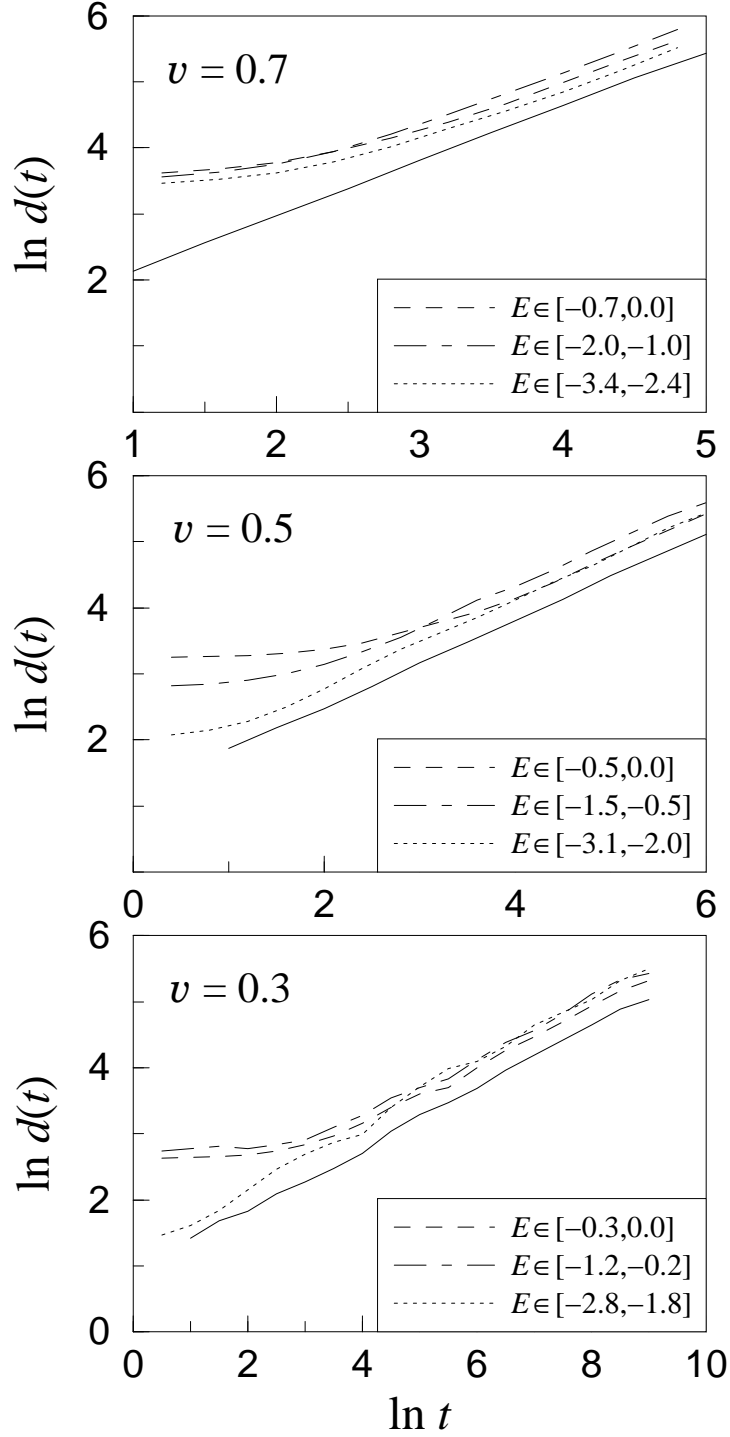


FIG. 9. The dependence of mean square displacement $d(t)$ on various energy windows. The energy windows are arbitrarily chosen from the band center (dashed line), the band edge (dotted line) and between the band center and the band edge (dot-dashed line), respectively. The solid line is the result for the full spectrum.

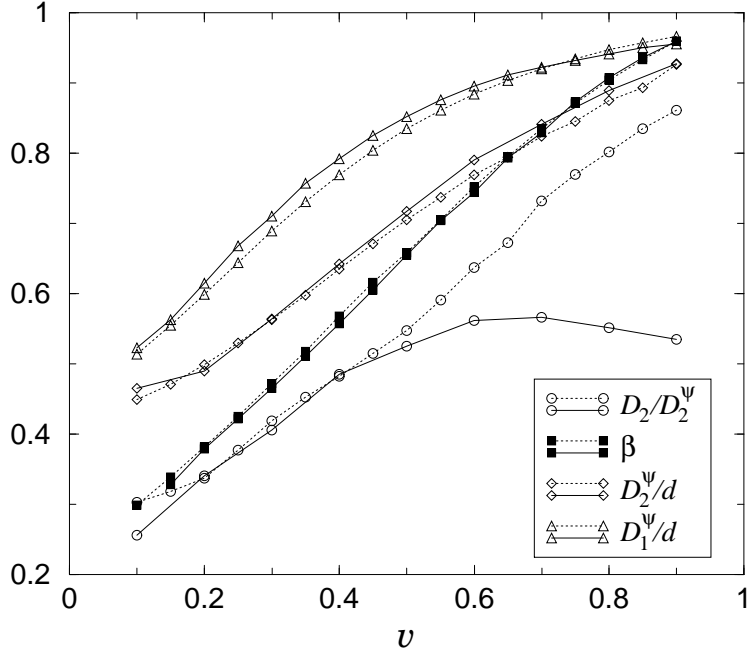


FIG. 10. The exponent β compared to several quantities describing the multifractal properties of the energy spectra and wavefunctions. The lines are included to guide the eye; the dotted lines correspond to the results for the octonacci chain ($d = 1$), the solid lines to the labyrinth tiling ($d = 2$).